Effective g-factor tensor for carriers in IV-VI semiconductor quantum wells

E. Ridolfi,[1] E. A. de Andrada e Silva,[2] and G. C. La Rocca[3]

[1]*Instituto de Física, Universidade Federal Fluminense, 24210-346 Niterói, Rio de Janeiro, Brazil*

[2]*Instituto Nacional de Pesquisas Espaciais, Caixa Postale 515, 12201-970 São José dos Campos, São Paulo, Brazil*

[3]*Scuola Normale Superiore and CNISM, Piazza dei Cavalieri 7, I-56126 Pisa, Italy*

(Received 8 December 2014; published 27 February 2015)

A theory for the electron (and hole) g factor in multivalley lead-salt IV-VI semiconductor quantum wells (QWs) is presented. An effective Hamiltonian for the QW electronic states in the presence of an external magnetic field is introduced within the envelope-function approximation, based on the multiband kp Dimmock model for the bulk. The mesoscopic spin-orbit (Rashba-type) and Zeeman interactions are taken into account on an equal footing and the effective g factor in symmetric quantum wells ($g^*_{\rm QW}$) is calculated analytically for each nonequivalent conduction-band (and valence-band) valley, and for QWs grown along different crystallographic directions.

DOI: 10.1103/PhysRevB.91.085313 PACS number(s): 73.21.−b, 73.21.Fg, 75.70.Tj

I. INTRODUCTION

Since the development of the first semiconductor electronic devices the lead-salt IV-VI semiconductor compounds have attracted great interest both for their applications (as narrow and direct gap materials for infrared lasers and detectors) and for the interesting relativistic physics involved in their electronic properties [1]. For example, the spin-orbit (SO) interaction in these compounds is particularly strong and is directly responsible for the opening of the fundamental gap in the bulk [2], as well as for the pure Rashba splitting in asymmetric quantum wells (QWs) [3]. IV-VI semiconductor nanostructures have been successfully fabricated and applied to different electronic devices [4–7]. More recently they have been at the center of the research on the physics of topological insulators and new spintronic devices [8,9].

However, the electronic structure of the IV-VI nanostructures, specially in the presence of a magnetic field, is not well known. In particular, the quantum confinement effects on the g factor of the carriers (electrons and holes) are not well understood and form the main focus of the present contribution. Within the multiband envelope function approximation, we present a simple theory for the electronic states of IV-VI QWs in the presence of a magnetic field, with analytical results for the g-factor tensor, as a function of both growth and magnetic field directions. The approach recently introduced to describe the g factor of carriers confined in III-V QWs [10] is here extended to the case of multivalley and anisotropic semiconductor structures. This work extends also the simplified theory in Ref. [11] which is based on a mini-kp approach and is specific for a longitudinal magnetic field and longitudinal valley in a [111] QW.

We recall that the g factor is a fundamental physical quantity which determines the spin splitting of the electronic states in response to an external magnetic field (Zeeman effect). Due to band-structure effects, for electrons (or quasiparticles) in a semiconductor, the corresponding g factor is renormalized from the bare value 2 and is referred to as the effective g factor (g^*), in analogy with the effective mass m^*. In a QW, g^* is further renormalized by the confining potential, can be tuned, and is a main parameter for spintronic applications. Here we discuss the physics of such mesoscopic g-factor renormalization in the case of IV-VI PbTe-like QWs.

II. EFFECTIVE HAMILTONIAN

We first derive an effective Hamiltonian for the electronic states starting from the Dimmock kp model for the bulk [2]. Considering the four equivalent valleys at the L point as independent of each other and using a coordinate system with the z axis along the main axis of the ellipsoidal valley, the conduction (or valence) band can be described by the following (energy-dependent) effective 2×2 Hamiltonian [12,13]:

$$H_{\rm eff}=\left[\frac{E_g}{2}+P_\parallel^2\hat{k}_z\gamma\hat{k}_z+P_\perp^2\hat{k}_x\gamma\hat{k}_x+P_\perp^2\hat{k}_y\gamma\hat{k}_y\right]+H_{\rm SO}, \tag{1}$$

with

$$\begin{aligned}H_{\rm SO}=&P_\parallel P_\perp(\gamma[\hat{k}_y,\hat{k}_z]+[\hat{k}_y,\gamma]\hat{k}_z-[\hat{k}_z,\gamma]\hat{k}_y)i\sigma_x\\&+P_\parallel P_\perp(\gamma[\hat{k}_z,\hat{k}_x]+[\hat{k}_z,\gamma]\hat{k}_x-[\hat{k}_x,\gamma]\hat{k}_z)i\sigma_y\\&+P_\perp^2(\gamma[\hat{k}_x,\hat{k}_y]+[\hat{k}_x,\gamma]\hat{k}_y-[\hat{k}_y,\gamma]\hat{k}_x)i\sigma_z,\end{aligned} \tag{2}$$

$\gamma=1/(E+\frac{E_g}{2})$, and, where the energy origin was set at the middle of the gap (of width E_g), x and y are the transverse directions, $\vec{\sigma}$ the Pauli matrices vector, $P_\parallel$ ($P_\perp$) the usual kp momentum matrix element parallel (perpendicular) to the valley main axis, and $(\hat{k}_x,\hat{k}_y,\hat{k}_z)$ the electron wave-vector operator. Note that $H_{\rm eff}$ is the Dimmock four-band model projected into the conduction band and that it is written in a form which facilitates the inclusion of both the magnetic field and the band-gap variation in a QW structure. Note also that in the bulk (and zero field), γ is constant, the envelope function is simply $e^{i\vec{k}\cdot\vec{r}}$, the k-vector components are c numbers, and all commutators above are equal to zero, so that one obtains the well-known nonparabolic dispersion relation around the gap of these narrow-gap semiconductors, described by the energy-dependent effective masses $m_{\parallel,\perp}=\frac{\hbar^2}{2P^2_{\parallel,\perp}}(E+\frac{E_g}{2})$, i.e.,

$$E=\frac{E_g}{2}+\frac{\hbar^2}{2}\left(\frac{k_\parallel^2}{m_\parallel(E)}+\frac{k_\perp^2}{m_\perp(E)}\right), \tag{3}$$

where $k_\perp^2=k_x^2+k_y^2$. In addition to the energy gap E_g, the only parameters are $P_\parallel$ and $P_\perp$, which are fixed with the measured band-edge effective mass $m^*_{\parallel,\perp}$, i.e., $P_{\parallel,\perp}=\sqrt{\hbar^2E_g/2m^*_{\parallel,\perp}}$, and are assumed constant along the QW structure in the

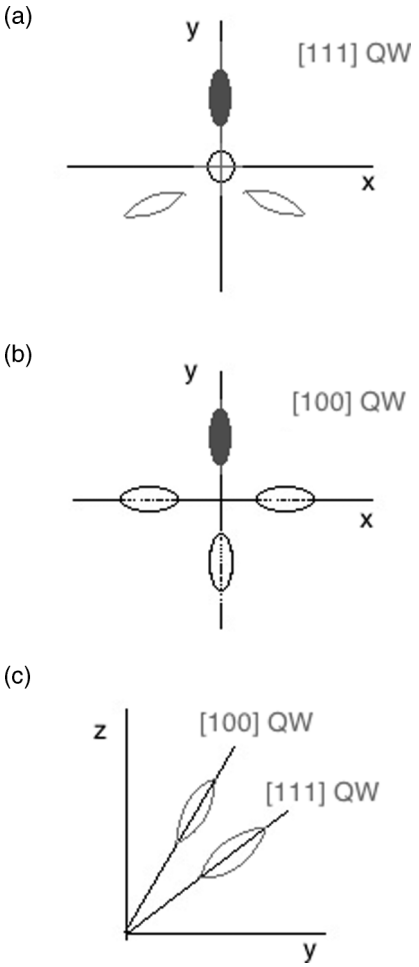

FIG. 1. Schematic illustration of the QW coordinate system, of the L valleys projected into the QW plane for growth direction (z) along both (a) [111] and (b) [100] crystallographic directions and (c) of the oblique valley (the solid symbol) orientation.

envelope function approximation. A specular equation is similarly obtained for the valence band. Such a model has been shown to describe very well the band structure of the lead salts near the fundamental band gap and is here used to study the QW in a $\vec{B}$-field problem.

In a QW the lack of translation symmetry along the growth direction, in general, breaks the valley degeneracy, and it is convenient to use a new coordinate system where now the z axis is along the growth direction (which, except for the longitudinal valley in a [111] QW, is not parallel to the valley main axis; see Fig. 1). So $E_g = E_g(z)$ and therefore $\gamma = \gamma(z)$ [the center of the band gap is also allowed to vary along the growth direction due to the band offset described by a step function $Q(z)$]. In the cases of interest, such a new QW coordinate system is obtained from the valley system used above with a simple rotation around a transverse direction (x), so that the components of a vector $\vec{v}$ are given by $v_x = v_{x'}$, $v_y = v_{y'}\cos(\theta) + v_{z'}\sin(\theta)$, and $v_z = v_{z'}\cos(\theta) - v_{y'}\sin(\theta)$, where θ is the angle of rotation and the valley system is now denoted by (x',y',z'), as sketched in Fig. 1.

III. QUANTUM-WELL EFFECTIVE g-FACTOR TENSOR

In order to include the effects of an external magnetic field $\vec{B}$, one then adds the Zeeman term of the bulk, i.e., $\frac{1}{2}\mu_0[g_\parallel B_{z'}\sigma_{z'} + g_\perp(B_{x'}\sigma_{x'} + B_{y'}\sigma_{y'})]$, where $g_\parallel$ and $g_\perp$ are the g-factor Dimmock parameters for the bulk conduction-band valleys, which (as for the effective masses) are fixed with the measured band-edge g factor $g^*_{\parallel,\perp}$, and makes also the fundamental substitution $\hat{k} \to \hat{k} + (e/\hbar)\vec{A} = -i\nabla + (e/\hbar)\vec{A}$, in the k-vector operator.

Following the classic work by Stern and Howard [14], we use the gauge $\vec{A} = (B_y z - B_z y, -B_x z, 0)$, set the envelope function as $\mathcal{F}(\vec{r}) = e^{ik_x x}F(y,z)$ (since $H_{\rm eff}$ does not depend on x), perform the unitary transformation defined by

$$F = e^{-iD(\hat{k}_y z - b_x z^2/2)} f$$

with

$$D = D(\theta) = \frac{(P_\parallel^2 - P_\perp^2)\sin(\theta)\cos(\theta)}{P_\parallel^2\cos(\theta)^2 + P_\perp^2\sin(\theta)^2}$$

in order to eliminate the term linear in $\hat{k}_y$, and use also the translation operator property

$$e^{ia\hat{k}_y} f(y) = f(y+a)e^{ia\hat{k}_y}.$$

After simple algebra, one obtains the following effective Hamiltonian (as a sum of kinetic, mesoscopic potential, Zeeman, and Rashba terms):

$$H_{\rm eff} = H_{\rm ki} + V(z) + H_{\rm Z} + H_{\rm R}, \tag{4}$$

where $V(z) = E_g(z)/2 + Q(z)$,

$$H_{\rm ki} = \frac{\hbar^2}{2}\left[\hat{k}_z\frac{1}{m_3}\hat{k}_z + \frac{(\hat{k}_y - b_x z)^2}{m_2} + \frac{(k_x + b_y z - b_z(y + Dz))^2}{m_1}\right] \tag{5}$$

(with $\vec{b} = (e/\hbar)\vec{B}$, $m_1 = m_\perp$, $m_2 = \cos(\theta)^2 m_\perp + \sin(\theta)^2 m_\parallel$, and $m_3 = m_\parallel m_\perp/(m_\perp\cos(\theta)^2 + m_\parallel\sin(\theta)^2)$), where the energy and z-dependent effective masses are given by

$$m_{\parallel,\perp}(E,z) = \frac{\hbar^2}{2P^2_{\parallel,\perp}}\left(E + \frac{E_g(z)}{2} - Q(z)\right), \tag{6}$$

the Zeeman term

$$H_{\rm Z} = \frac{\mu_0}{2}\vec{B}\times\left[\tilde{g}_0 + \frac{4m_e}{\hbar^2}(\gamma_{\rm SO}\tilde{g}_{\rm SO} + z\frac{\partial\gamma_{\rm SO}}{\partial z}\tilde{g}_{\rm QW})\right]\vec{\sigma}\,, \tag{7}$$

where the $\tilde{g}$s are the components of the effective g-factor tensor (given below) and

$$\gamma_{\rm SO} = \frac{P_\parallel P_\perp}{E + \frac{E_g(z)}{2} - Q(z)}\,;$$

finally

$$H_{\rm R} = \left(\frac{\partial\gamma_{\rm SO}}{\partial z}\right)\vec{B}_{\rm R}(k_x,\hat{k}_y)\times\vec{\sigma}\,, \tag{8}$$

with the effective k-dependent Rashba field given by

$$\vec{B}_{\rm R} = (-\hat{k}_y, (rs^2 + c^2)k_x, (r-1)sck_x),$$

where, to simplify, we use $c = \cos(\theta)$, $s = \sin(\theta)$, and the anisotropy parameter

$$r = \frac{P_\perp}{P_\parallel} = \sqrt{\frac{m^*_\parallel}{m^*_\perp}}.$$

As the main result, one gets the QW effective g-factor tensor [Eq. (7)] given by the following three components:

$$\tilde{g}_0 = \begin{pmatrix} g_\perp & 0 & 0 \\ 0 & g_\perp c^2 + g_\parallel s^2 & (g_\parallel - g_\perp)sc \\ 0 & (g_\parallel - g_\perp)sc & g_\perp s^2 + g_\parallel c^2 \end{pmatrix}, \tag{9}$$

$$\tilde{g}_{\rm SO} = \begin{pmatrix} 1 & 0 & 0 \\ 0 & rs^2 + c^2 & (r-1)sc \\ 0 & (r-1)sc & rc^2 + s^2 \end{pmatrix}, \tag{10}$$

and

$$\tilde{g}_{\rm QW} = \begin{pmatrix} 1 & 0 & 0 \\ 0 & rs^2 + c^2 & (r-1)sc \\ 0 & -(rs^2 + c^2)\left(\frac{\gamma}{z} + D\right) & -(r-1)sc\left(\frac{\gamma}{z} + D\right) \end{pmatrix}. \tag{11}$$

For example, the result for the bulk is simply recovered by noting that in this case $\gamma_{\rm SO}$ is constant and, in the valley coordinate system (i.e., with $c = 1$ and $s = 0$), one then has

$$\tilde{g}_{\rm bulk} = \begin{pmatrix} g^*_\perp & 0 & 0 \\ 0 & g^*_\perp & 0 \\ 0 & 0 & g^*_\parallel \end{pmatrix}, \tag{12}$$

with

$$g^*_\perp = g_\perp + \frac{4m_e}{\hbar^2}\gamma_{\rm SO} \tag{13}$$

and

$$g^*_\parallel = g_\parallel + \frac{4m_e}{\hbar^2}\gamma_{\rm SO} r, \tag{14}$$

which are energy dependent and can also be written as a function of the above-defined parallel and perpendicular effective masses, i.e.,

$$g^*_\perp(E) = g_\perp + \frac{2m_e}{\sqrt{m_\perp(E)m_\parallel(E)}}$$

and

$$g^*_\parallel(E) = g_\parallel + \frac{2m_e}{m_\perp(E)}.$$

Note that the Dimmock parameters $g_\perp$ and $g_\parallel$ correspond to the remote bands contribution (including the bare electron g-factor value $\sim$2) and that the III-V-like spherical symmetric case is obtained only with $g_t = g_l$ and $r = 1$.

It is the third term in H_z above, proportional to $\frac{\partial \gamma_{\rm SO}}{\partial z}$, that gives the QW contribution due to the mesoscopic quantum confinement. As shown in Ref. [10] for GaAs QWs, the QW effective g factor ($g^*_{\rm QW}$) can conveniently be calculated with perturbation theory. Using the ground state of $H_0 = H_{ki}(\vec{B} = 0) + V(z)$, one simply calculates $\langle f_0|H_Z|f_0\rangle = \bar{H}_z$, where $H_0 f_0 = E_0 f_0$. Next, following the same scheme, we consider the lead-salt QW effective g factors for different growth directions and nonequivalent valleys. Such an approach for the calculation of $g^*_{\rm QW}$ is simpler and more transparent than that used before for the L-valley electrons in SiGe QW structures [15].

IV. [111], [100], AND [110] QUANTUM WELLS

We now consider common symmetric QWs grown along the [111] and [100] crystallographic directions and with interfaces at $z = \pm L/2$. For [111] QWs, the four equivalent L valleys in the bulk split into one longitudinal and three oblique ones, while for [100] QWs we deal with four degenerate oblique valleys (see Fig. 1). In the expressions above, all one has to do is to set ($s = 0$, $c = 1$) for the longitudinal valley and for the oblique valleys ($s = 2\sqrt{2}/3$, $c = 1/3$) for [111] QWs and ($s = \sqrt{2/3}$, $c = 1/\sqrt{3}$) for [100] QWs. The applied magnetic field is considered both longitudinal (along the growth direction) and transverse (in the QW plane) and the corresponding effective g factors $g^*_{\rm QW,l}$ and $g^*_{\rm QW,t}$ are calculated.

For the numerical results and illustrative examples, PbSnTe/PbTe QWs are considered with the following low-temperature empirical parameters: $E_g^{\rm PbTe} = 0.19$ eV, $m^{*,\rm PbTe}_\parallel = 0.24m_e$, $m^{*,\rm PbTe}_\perp = 0.024m_e$ [12], $g^{*(\rm PbTe)}_\parallel = 58$, $g^{*(\rm PbTe)}_\perp = 15$ [16,17], and $E_g^{\rm PbSnTe} = 0.1$ eV. The Dimmock parameters $g_\parallel$ (=−24.3) and $g_\perp$ (=−11.4) are determined by $g^{*(\rm PbTe)}_\parallel$ and $g^{*(\rm PbTe)}_\perp$, respectively, and assumed constant along the structure. A symmetrical 0.5 band offset is used. The unperturbed ground-state energy E_i and corresponding envelope function $f_0 = f_i(z)$ for each nonequivalent valley, i.e., with $i = 1$ (longitudinal) or $i = $ o (oblique), are calculated exactly following standard procedure as described in Refs. [10,12].

A. Longitudinal valley

For the longitudinal valley and longitudinal magnetic field $\vec{B} = B\hat{z}$ one gets the QW effective g factor simply given by the bulk average, in perfect analogy to the III-V case, i.e.,

$$g^*_{\rm QW,l} = \langle g^*_\parallel \rangle = g^*_{\parallel,\rm w}(E_1)P_{\rm w} + g^*_{\parallel,\rm b}(E_1)P_{\rm b}, \tag{15}$$

where P_j ($=\int_j |f_l(z)|^2 dz$) is the probability to find the electron in the well ($j =$ w) or in the barrier ($j =$ b) (note that for the longitudinal valley $D = 0$ so that for the longitudinal field, there is no QW or interface contribution, i.e., from $\tilde{g}_{\rm QW}$). To simplify the notation, from now on, as above, the energy-dependent parameters are meant to be calculated at E_1 or at $E_{\rm o}$ depending on whether it is a longitudinal or an oblique valley effective QW g factor (similarly, f_0 stands for either f_1 or $f_{\rm o}$).

In Fig. 2, $g^*_{\rm QW,l}$ for electrons (or holes) in PbSnTe/PbTe QWs is plotted as a function of the well width. For comparison and as limiting cases, the energy-dependent bulk g factors for both PbTe and PbSnTe are also plotted. See for instance that as expected $g^*_{\rm QW,l}$ tends to the well bulk value and to the barrier (PbTe) bulk value in the limits of L going to infinity and to zero, respectively. Note also that these bulk energy-dependent g factors decrease with increasing quantum confinement, as opposed to the behavior observed in the III-V QW case.

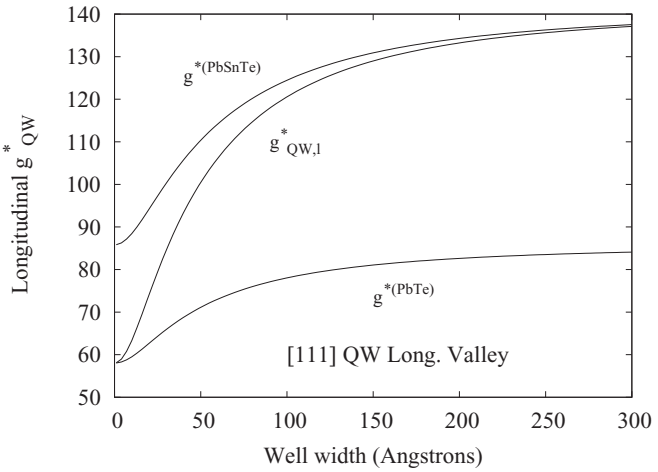

FIG. 2. Effective g factor for the longitudinal valley electrons in PbSnTe/PbTe [111] QWs and longitudinal B field (along the growth direction) as a function of the well width. The limiting (well and barrier) energy-dependent bulk effective g factors are also plotted, giving the effect of the QW confinement energy shift.

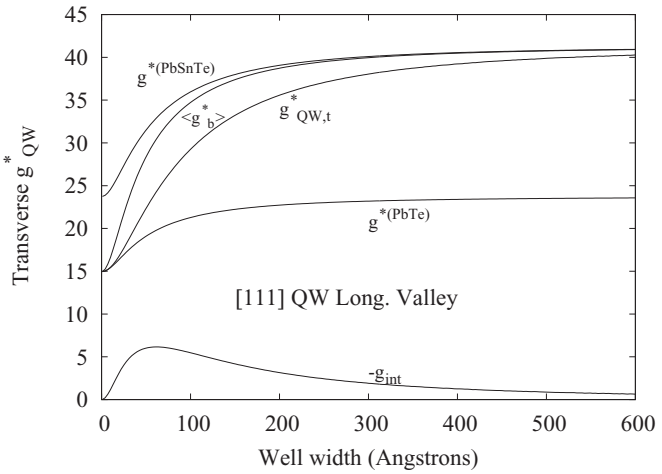

FIG. 3. Effective g factor for the longitudinal valley electrons in PbSnTe/PbTe [111] QWs and transverse magnetic field $g^*_{\mathrm{QW,t}}$ as a function of the well width. For the different contributions to QW g-factor renormalization (i.e., barrier penetration, confinement energy shift, and interface SO contributions), the energy-dependent barrier and well g factors, as well as the average bulk g factor, showing the wave-function barrier penetration effect, are also plotted.

For a transverse B field, again analogous to the III-V QW case, one gets

$$g^*_{\mathrm{QW,t}} = \langle g^*_\perp \rangle + \frac{4m_e}{\hbar^2}\left\langle z\frac{\partial \gamma_{\mathrm{SO}}}{\partial z}\right\rangle, \tag{16}$$

which is the average bulk g factor plus an interface spin-orbit contribution g^*_{int} given by

$$g_{\mathrm{int}} = -\frac{4m_e}{\hbar^2}\,\delta\gamma_{\mathrm{SO}}\,L\,|f_0(L/2)|^2, \tag{17}$$

where $\delta\gamma_{\mathrm{SO}} = \gamma^{(w)}_{\mathrm{SO}} - \gamma^{(b)}_{\mathrm{SO}}$. Recall that γ_{SO} is a step function in z changing from $\gamma^{(w)}_{\mathrm{SO}}$ to $\gamma^{(b)}_{\mathrm{SO}}$ at the interface; $|f_0(L/2)|^2 = |f_0(-L/2)|^2$ was also used. As in the III-V QW case, the IV-VI longitudinal valley $g^*_{\mathrm{QW,t}}$ does not depend on the B-field direction in the plane; therefore, the g-factor anisotropy $\Delta g^*_{\mathrm{QW}} = g^*_{\mathrm{QW,l}} - g^*_{\mathrm{QW,t}}$ in this case is simply given by

$$\Delta g^*_{\mathrm{QW}} = \langle g^*_\parallel - g^*_\perp \rangle - g_{\mathrm{int}}. \tag{18}$$

Different from the III-V QW case, such IV-VI g-factor anisotropy presents two contributions: a bulk average and an interface one determined by the mesoscopic (Rashba-type) spin-orbit interaction. Figure 3 shows the well width dependence of such $g^*_{\mathrm{QW,t}}$ in a PbSnTe/PbTe QW. To compare and access the different contributions to the QW g factor, which include wave-function barrier penetration, confinement energy shift, and interface SO interaction, the energy-dependent bulk g factors and their average are also plotted. Note that in the shallow wells here considered the interface contribution to the g factor (g_{int}) decays slowly with increasing well width.

B. Oblique valleys

For the oblique valleys instead the transverse g factor does depend on the B-field direction in the QW plane. The transverse magnetic field actually breaks the oblique valley degeneracy, while the longitudinal field (i.e., along the growth direction) does not. Considering the specific oblique valley which sets the valley system in the above-used coordinate-system rotation, for the longitudinal $\vec{B} = B\hat{z}$ one gets

$$\langle g_0|H_z|g_0\rangle = \frac{\mu_0}{2}B(g^*_{zy}\sigma_y + g^*_{zz}\sigma_z), \tag{19}$$

with

$$g^*_{zy} = sc\langle g^*_\perp - g^*_\parallel\rangle - (s^2r + c^2)D\,g_{\mathrm{int}} \tag{20}$$

and

$$g^*_{zz} = \langle s^2\,g^*_\perp + c^2\,g^*_\parallel\rangle - sc\,(r-1)\,D\,g_{\mathrm{int}}. \tag{21}$$

Noting that $D = 2\sqrt{2}(1-r^2)/(1+8r^2)$ for [111] and $D = \sqrt{2}(1-r^2)/(1+2r^2)$ for [100] QWs we then have explicitly

$$g^*_{zy} = \frac{2\sqrt{2}}{9}\left[\langle g^*_\perp - g^*_\parallel\rangle - \frac{(8r+1)(1-r^2)}{8r^2+1}\,g_{\mathrm{int}}\right], \tag{22}$$

$$g^*_{zz} = \frac{\langle 8g^*_\perp + g^*_\parallel\rangle}{9} - \frac{8}{9}\frac{(r-1)(1-r^2)}{8r^2+1}\,g_{\mathrm{int}}, \tag{23}$$

for [111] QWs, and

$$g^*_{zy} = \frac{\sqrt{2}}{3}\left[\langle g^*_\perp - g^*_\parallel\rangle - \frac{(2r+1)(1-r^2)}{2r^2+1}\,g_{\mathrm{int}}\right], \tag{24}$$

$$g^*_{zz} = \frac{\langle 2\,g^*_\perp + g^*_\parallel\rangle}{3} - \frac{2}{3}\frac{(r-1)(1-r^2)}{2r^2+1}\,g_{\mathrm{int}}, \tag{25}$$

for [100] QWs.

Due to the anisotropy ($r \neq 1$), the oblique valleys are seen to present an interface contribution to their effective g factor even for a longitudinal magnetic field. In these structures, contrary to the III-V QW case [10], such a longitudinal field does not drive the electrons along a purely transverse cyclotron orbit in real space. As a matter of fact, due to the valley anisotropy, the electron velocity $\vec{v} = \frac{1}{\hbar}\nabla_{\vec{k}}E(\vec{k})$ has in general a component along the magnetic field even when $\vec{k}$ remains perpendicular to

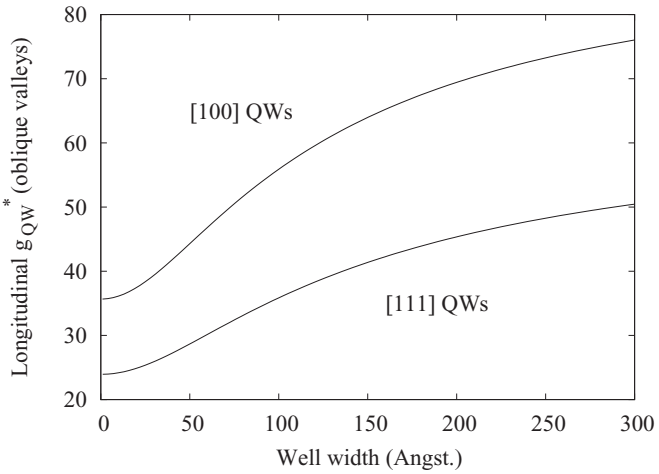

FIG. 4. Longitudinal effective g factor for the oblique valley electrons in PbSnTe/PbTe [111] and [100] QWs as a function of the well width.

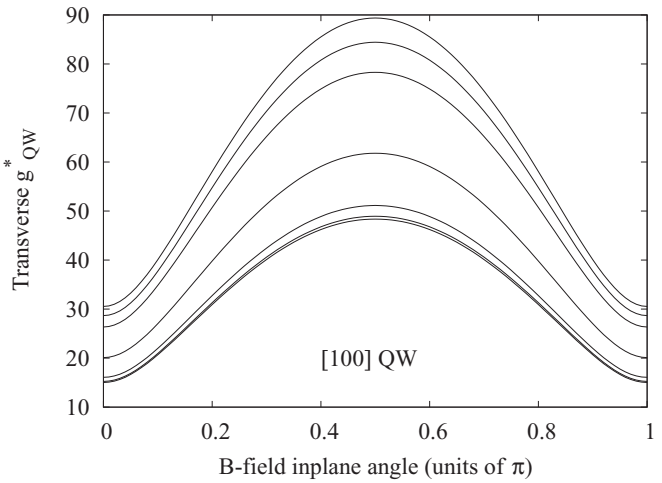

FIG. 5. Transverse effective g factor for the oblique valley electrons in PbSnTe/PbTe [100] QWs, as a function of the in-plane B-field angle (with respect to $\hat{x}$) and for different well widths $L = 1$, 2, 4, 10, 20, 25, and 30 nm from the bottom to the top.

$\vec{B}$. Again when $g_\perp = g_\parallel$ and $r = 1$ the symmetrical III-V like result is recovered. In Fig. 4, as a function of the PbSnTe/PbTe QW width, the resulting longitudinal effective g factor for the oblique valleys in both [111] and [100] QWs is plotted, given by

$$g^*_{\mathrm{o,l}} = \sqrt{g^{*2}_{zy} + g^{*2}_{zz}}$$

and which determines the Zeeman splitting ΔE ($=\mu_0 B g^*_{\mathrm{o,l}}$). Comparing Eqs. (22) and (23) for [111] QWs with Eqs. (24) and (25) for [100] QWs, one can see that the larger g factor obtained in the latter case is due to a larger weight of $g^*_\parallel$, which is larger than $g^*_\perp$ [see also sketch in Fig. 1(c)].

The last and most anisotropic situation is that of the oblique valleys with a transverse B field, where the crystal growth, the magnetic field, and the valley main axis are each along a different direction; indeed in this case one gets

$$\langle H_z \rangle = \frac{\mu_0}{2} B[\cos(\phi) g^*_{xx}\sigma_x + \sin(\phi)(g^*_{yy}\sigma_y + g^*_{yz}\sigma_z)], \quad (26)$$

where ϕ is the in-plane angle between $\vec{B}$ and $\hat{x}$,

$$g^*_{xx} = \langle g^*_\perp \rangle + g_{\mathrm{int}} \quad (27)$$

[equal to the above longitudinal valley $g^*_{\mathrm{QW,t}}$ except that here, as mentioned, the average of the bulk and the interface contribution g_{int} [Eq. (17)] is calculated with the oblique valley unperturbed energy and envelope function] and

$$g^*_{yy} = [\langle g^*_\perp + 8\, g^*_\parallel \rangle + (8\, r + 1)\, g_{\mathrm{int}}]/9, \quad (28)$$

$$g^*_{yz} = 2\sqrt{2}[\langle g^*_\parallel - g^*_\perp \rangle + (r - 1)\, g_{\mathrm{int}}]/9\,, \quad (29)$$

for [111] QWs, and

$$g^*_{yy} = [\langle g^*_\perp + 2\, g^*_\parallel \rangle + (2\, r + 1)\, g_{\mathrm{int}}]/3, \quad (30)$$

$$g^*_{yz} = \sqrt{2}[\langle g^*_\parallel - g^*_\perp \rangle + (r - 1)\, g_{\mathrm{int}}]/3\,, \quad (31)$$

for [100] QWs.

As an example, Fig. 5 shows the obtained oblique valley transverse effective g factor

$$g^*_{\mathrm{o,t}} = \sqrt{\cos(\phi)^2 g^{*2}_{xx} + \sin(\phi)^2 \left(g^{*2}_{yy} + g^{*2}_{yz}\right)}$$

for [100] PbSnTe/PbTe, as a function of ϕ and for different well widths. For [111] QWs one obtains very similar results, with slightly smaller values (a difference much smaller than that in Fig. 4 for the longitudinal field case). With varying L we see the crossover between the bulk anisotropy in PbTe and that in PbSnTe that give the limits of very small and very large L, respectively.

To conclude it is interesting to note that a pure mesoscopic g-factor anisotropy in IV-VI QWs can be seen with the so-called transverse valleys in [110] QWs. In these QWs the four L valleys split into two with the main axis in the QW plane, the transverse ones, and two oblique ones. For the transverse valleys we put $c = 0$ and $s = 1$ and for longitudinal magnetic fields (i.e., along [110] $\parallel \hat{z}$) we get

$$g^*_{\mathrm{QW,l}} = \langle g^*_\perp \rangle,$$

while for transverse B fields

$$g^*_{\mathrm{QW,t}} = \sqrt{\mathcal{C}^2(\langle g^*_\perp \rangle + g_{\mathrm{int}})^2 + \mathcal{S}^2(\langle g^*_\parallel \rangle + r\, g_{\mathrm{int}})^2},$$

where $\mathcal{C} = \cos(\phi)$ and $\mathcal{S} = \sin(\phi)$ with ϕ, as before, giving the direction of the magnetic field in the QW plane. So that if one rotates $\vec{B}$ from $\hat{z}$ to $\hat{x}$ ($\phi = 0$) one gets

$$\Delta g^*_{\mathrm{QW}} = g^*_{\mathrm{QW,t}} - g^*_{\mathrm{QW,l}} = g_{\mathrm{int}},$$

with a maximum of $\Delta g^*_{\mathrm{QW}} = 5.3$ at $L = 13.8$ nm (the well width dependence is similar to that shown in the bottom curve of Fig. 3).

V. CONCLUSIONS

Summarizing, an envelope-function theory for the electronic structure of IV-VI semiconductor QWs in an external magnetic field has been presented, with analytical results for

the electron (or hole) effective g-factor tensor. Specific results for QWs grown along [111], [100], and [110] crystallographic directions and magnetic field along all directions are discussed. The effective g factor in these structures is seen to be renormalized by the confining mesoscopic potential through the Rashba-type spin-orbit coupling. The results are compared to the known III-V QW case and many differences are pointed out. In particular the effective g factor for electrons confined in IV-VI QWs is shown to be highly anisotropic not only due to the magnetic field direction (with respect to the QW growth direction) but also due to the misalignment between the L-valley main axis and the growth direction, and to the IV-VI L-valley intrinsic anisotropy. The obtained expressions for the effective g-factor tensor are general and can be applied to QWs made of any lead-salt (IV-VI) compound grown along different directions, and should be useful also for spintronic applications.

ACKNOWLEDGMENTS

E.A.A.S. is thankful to the Scuola Normale Superiore di Pisa for the kind hospitality. Support from the Brazilian agencies FAPESP (Grant No. 2014/09878-1), CNPq (Grant No. 455097/2013-5), and CAPES is also acknowledged.

[1] P. Yu and M. Cardona, *Fundamentals of Semiconductors* (Springer, New York, 2001).
[2] J. O. Dimmock, *Physics of Semimetals and Narrow-Gap Semiconductors,* edited by D. L. Carter and R.T. Bate (Pergamon, New York, 1971), p. 319.
[3] M. M. Hasegawa and E. A. de Andrada e Silva, Phys. Rev. B **68**, 205309 (2003).
[4] E. Abramof, E. A. de Andrada e Silva, S. O. Ferreira, P. Motisuke, P. H. O. Rappl, and A. Y. Ueta, Phys. Rev. B **63**, 085304 (2001).
[5] P. McCann, *Mid-infrared Semiconductor Optoelectronics*, Springer Series in Optical Sciences Vol. 118, edited by A. Krier (Springer, New York, 2006), p. 237.
[6] G. Springholz and G. Bauer, Phys. Status Solidi B **244**, 2752 (2007).
[7] L. Elizondo, P. J. McCann, S. Elizondo, and S. Shi, *IV-VI Semiconductor Nanostructures: Physics and Applications* (VDM Verlag, Saarbrücken, Germany, 2009).
[8] R. Buczko and L. Cywiński, Phys. Rev. B **85**, 205319 (2012).
[9] M. Z. Hasan and C. L. Kane, Rev. Mod. Phys. **82**, 3045 (2010).
[10] M. A. Toloza Sandoval, A. Ferreira da Silva, E. A. de Andrada e Silva, and G. C. La Rocca, Phys. Rev. B **86**, 195302 (2012).
[11] V. K. Dugaev and P. P. Petrov, Phys. Status Solidi B **184**, 347 (1994).
[12] E. A. de Andrada e Silva, Phys. Rev. B **60**, 8859 (1999).
[13] E. Ridolfi, Dissertation, Universitá di Pisa, Pisa, Italy, 2013.
[14] F. Stern and W. E. Howard, Phys. Rev. **163**, 816 (1967).
[15] F. A. Baron, A. A. Kiselev, H. D. Robinson, K. W. Kim, K. L. Wang, and E. Yablonovitch, Phys. Rev. B **68**, 195306 (2003).
[16] H. Schaber and R. Doezema, Solid State Commun. **31**, 197 (1979).
[17] T. Ichiguchi, S. Nishikawa, and K. Murase, Solid State Commun. **34**, 309 (1980).